

PAPER • OPEN ACCESS

Impact of tropical teleconnections on the long-range predictability of the atmosphere at midlatitudes: a reduced-order multi-scale model perspective

To cite this article: Stéphane Vannitsem 2023 *J. Phys. Complex.* **4** 045006

View the [article online](#) for updates and enhancements.

You may also like

- [Salient difference of sea surface temperature over the North Atlantic in the spring following three super El Niño events](#)
Jinhua Yu, Xuyu Zhang, Laurent Li et al.
- [Dynamics of Massive Atmospheres](#)
Rei Chemke and Yohai Kaspi
- [Tropical influences on European summer climate variability](#)
Anna Maidens and Jeff R Knight



PAPER

OPEN ACCESS

RECEIVED
24 May 2023REVISED
9 October 2023ACCEPTED FOR PUBLICATION
19 October 2023PUBLISHED
1 November 2023

Original Content from
this work may be used
under the terms of the
[Creative Commons
Attribution 4.0 licence](#).

Any further distribution
of this work must
maintain attribution to
the author(s) and the title
of the work, journal
citation and DOI.



Impact of tropical teleconnections on the long-range predictability of the atmosphere at midlatitudes: a reduced-order multi-scale model perspective

Stéphane Vannitsem

Royal Meteorological Institute of Belgium, Avenue Circulaire 3, 1180 Brussels, Belgium

E-mail: Stephane.Vannitsem@meteo.be**Keywords:** teleconnections, low-frequency variability, ENSO, predictability, chaos

Abstract

Teleconnections between the tropical and the extratropical climates are often considered as a potential source of long-term predictability at seasonal to decadal time scales in the extratropics. This claim is taken up in the present work by investigating the predictability of a coupled ocean–atmosphere extratropical model under a one-way forcing generated by a tropical model. Both models display a chaotic dynamics, and the dominant variable of the extratropical model displays a high correlation with the tropical forcing in the reference simulation, inducing a low-frequency variability signal in the extratropics. Numerical experiments emulating the presence of initial condition errors in the tropical model are conducted to clarify their impact on the predictability in the extratropics. It is shown that: (i) the correlation skill of the dominant observable affected by the forcing is considerably degraded at interannual time scales due to the presence of initial condition errors in the tropics, limiting the potential of teleconnections; (ii) averaging of an ensemble of forecasts—with a small number of members—may substantially improve the quality of the forecasts; and (iii) temporal averaging may also improve the quality of the forecasts (at the expense of being able to forecast extreme events), in particular when the forcing affects weakly the observable under interest.

1. Introduction

The tropical regions display key low-frequency variability (LFV) ranging from months with the Madden–Julian Oscillation to annual and decadal time scales for the El-Niño–Southern Oscillation (ENSO). These processes display teleconnections with large regions in the extratropics as discussed in [1–5]. These are often expressed in terms of correlations between the tropical and extratropical regions, suggesting a potential influence on one another. Note however that correlation does not mean causation as already stressed in many recent works on causality analyses [6–9]. In [9], a new approach of causality detection was used to clarify the transfer of information among different climate indices and in particular ENSO on monthly to decadal time scales. It was in particular shown that ENSO has considerable influence on the Pacific North Atlantic pattern, on the Pacific decadal oscillation, on the tropical North Atlantic region and slightly on the Arctic oscillation. The mechanism often put forward for the teleconnections with the midlatitudes is the atmospheric bridge described in [2].

As these tropical processes have typical time scales of evolution much longer than the ones of the extratropical dynamics, it is natural to expect that these LFV signals would emerge in the evolution of the extratropical atmosphere, and could be exploited in seasonal and decadal forecasts of the midlatitude dynamics [10, 11], although the way these frequencies will emerge is a complicate matter as illustrated in [12]. But the processes developing in the tropical regions are not simple periodic signals that could be easily exploited as for instance the annual cycle. They display an erratic behavior reminiscent of chaotic or stochastically-forced dynamics [13]. This implies that these processes display the property of sensitivity to

initial conditions that will affect any forecast of the tropical evolution as initial state errors are always present in the model forecasts, and these uncertainties will, in turn, affect the evolution of the signal at midlatitudes.

The starting point of the present work is the claim that any forecast will hardly be able to exploit the full potential of teleconnections. This claim is demonstrated by investigating the impact of errors in the initial conditions of a tropical forcing on an extratropical model. This system has been recently built to investigate the emergence of pullback attractors in a midlatitude reduced-order coupled ocean–atmosphere model forced by a tropical low-order model [12]. The midlatitude model is the so-called Vannitsem–Demaeyer–DeCruz–Ghil (VDDG) model describing the interaction between a two-layer quasi-geostrophic atmosphere with a 1.5-layer quasi-geostrophic ocean [14], while the tropical low-order model is a box model developed by [13, 15, 16]. A one-way interaction is imposed from the tropical model to the extratropical one. The solutions of both models that will be used in the present work display chaotic dynamics, and are therefore sensitive to the initial conditions. The experiments that will be performed will be to introduce random initial state errors of different amplitudes in the tropical model to clarify the ability of the extratropical model to produce long-term skillful forecasts at midlatitudes.

In section 2, the coupled tropical–extratropical model setup is described, together with the parameter used in the current experiment and the reference solutions around which the predictability experiments will be performed. Section 3 is devoted to the description of the experimental setup and the analysis of the different experiments. The impact of ensemble averaging and temporal averaging are also explored in this section. The main conclusions are drawn in section 4.

2. Governing equations for the tropical–extratropical model

2.1. The ENSO module

The ENSO model was developed in a series of papers by Timmermann *et al* and colleagues [13, 15–18]. They modeled the dynamics of the ocean’s upper layer in the tropical Pacific using a low number of variables. Their ENSO model describes the dynamics of the temperature in the eastern and western tropical Pacific basins, completed by an equation for the evolution of the thermocline depth. The model represents the horizontal discharge–recharge mechanisms at play in the tropical Pacific through the heat exchanges between the tropical and subtropical waters, subject to surface wind stress and upwelling of subsurface cold water in the eastern part of the domain [16]. [18] developed a nondimensional model version in which the time is normalized by a typical time scale of tropical wave propagation of roughly 3.5 months. The latter ENSO model version is coupled here with an extratropical module whose time is nondimensionalized by the Coriolis parameter f_0 , and the [18] equations are therefore slightly modified in order to incorporate this change of reference time scale:

$$\frac{dx}{dt} = \rho\delta(x^2 - ax) + sx(x + y + c - c \tanh(x + z)), \quad (1a)$$

$$\frac{dy}{dt} = -\rho\delta(ay + x^2), \quad (1b)$$

$$\frac{dz}{dt} = \delta\left(k - z - \frac{x}{2}\right). \quad (1c)$$

Here x, y, z and t are dimensionless, x is the temperature difference between the eastern and western basins of the tropical Pacific, y the western basin’s temperature anomaly with respect to a reference value, and z the western basin’s thermocline depth anomaly.

The dimensionless parameters are defined as follows

$$a = \frac{\alpha b L}{\epsilon h \beta}, \quad \rho = \frac{\epsilon h \beta}{r b L}, \quad \delta = \frac{r}{f_0}, \quad (2a)$$

$$c = \frac{C}{S_0}, \quad k = \frac{K}{S_0}, \quad s = \frac{\zeta h \beta}{b L f_0}, \quad (2b)$$

with f_0 the Coriolis parameter used to nondimensionalize the time, and the other parameters as defined in [18, table 1]. For the applications presented in this paper, one set of parameter values is considered leading to a chaotic solution, see table 1.

The ENSO module is taken here to be unaffected by the midlatitude module, and is thus the driving system in the coupled tropical–extratropical model. Equation (1) can thus be integrated independently of the rest of the model, and this is done using a fourth-order Runge–Kutta scheme with a time step $\Delta t = 0.1346 \text{ h} = 0.05$ nondimensional time units. The variable $x + y$ corresponds in the model (1) to the sea surface temperatures in the eastern tropical Pacific that are commonly associated with the Niño-3 index, that

Table 1. Dimensionless parameter values of the ENSO module.

$a = 7.658\,609\,809$
$\rho = 0.290\,16$
$\delta = 0.000\,2803$
$c = 2.3952$
$k = 0.4032$
$s = 0.001\,069\,075$

will be referred later as T_{ENSO} . A long chaotic solution was started from the initial state ($x = -2.8439$, $y = -0.62$, $z = 1.480$) that will be used in the following as the long reference trajectory of the tropical dynamics.

2.2. The VDDG extratropical model

The coupled ocean–atmosphere model used herein for the midlatitudes was developed by [19] and it is called hereafter the VDDG model. Different versions of this model have been used to study LFV within the coupled ocean–atmosphere system [20, 21], to investigate the properties of the Lyapunov exponents in such a system [22, 23], to build the stochastic parametrization of subgrid-scale forcing [24, 25], and to develop data assimilation schemes in coupled models [26–28].

The atmospheric module is based on the vorticity equations of a two-layer quasi-geostrophic flow defined on a beta-plane [29, 30]. The equations in pressure coordinates are:

$$\frac{\partial}{\partial t} (\nabla^2 \psi_a^1) + J(\psi_a^1, \nabla^2 \psi_a^1) + \beta \frac{\partial \psi_a^1}{\partial x} = -k'_d \nabla^2 (\psi^1 - \psi^3) + \frac{f_0}{\Delta p} \omega, \quad (3a)$$

$$\frac{\partial}{\partial t} (\nabla^2 \psi_a^3) + J(\psi_a^3, \nabla^2 \psi_a^3) + \beta \frac{\partial \psi_a^3}{\partial x} = +k'_d \nabla^2 (\psi_a^1 - \psi_a^3) - \frac{f_0}{\Delta p} \omega - k_d \nabla^2 (\psi_a^3 - \psi_o). \quad (3b)$$

Here ψ_a^1 and ψ_a^3 are the streamfunction fields at 250 hPa and 750 hPa, respectively, while $\omega = dp/dt$ is the vertical velocity, f_0 the Coriolis parameter at $\phi_0 = 45^\circ$ latitude, and $\beta = df/dy$ at ϕ_0 . The coefficients k_d and k'_d multiply the surface friction term and the internal friction between the layers, respectively.

An additional term has been introduced in equation (3b) in order to account for the presence of a surface boundary velocity ψ_o of the oceanic flow; see equation (4) below. This term corresponds to the Ekman pumping on a moving surface and is the mechanical contribution of the interaction between the ocean and the atmosphere.

The ocean module is described by the reduced-gravity, quasi-geostrophic shallow-water model [29, 30]. The forcing is provided by the wind generated by the atmospheric module above. The governing equation is:

$$\frac{\partial}{\partial t} \left(\nabla^2 \psi_o - \frac{\psi_o}{L_R^2} \right) + J(\psi_o, \nabla^2 \psi_o) + \beta \frac{\partial \psi_o}{\partial x} = -r \nabla^2 \psi_o + \frac{\text{curl}_z \vec{\tau}}{\rho H}, \quad (4)$$

where ψ_o is the streamfunction, ρ the density of water, H the depth of the fluid layer, L_R the reduced Rossby deformation radius, r a Rayleigh friction coefficient at the bottom of the fluid layer, and $\text{curl}_z \vec{\tau}$ is the vertical component of the wind stress curl.

The wind stress in the VDDG model is given by $(\tau_x, \tau_y) = C(u - U, v - V)$, where $(u = -\partial \psi_a^3 / \partial y, v = \partial \psi_a^3 / \partial x)$ are the horizontal components of the geostrophic wind, and (U, V) the components of the geostrophic currents in the ocean. One thus gets

$$\text{curl}_z \tau = C \nabla^2 (\psi_a^3 - \psi_o). \quad (5)$$

and the wind stress is proportional to the relative velocity between the flow in the ocean's upper layer and the wind in the lower atmospheric layer. The drag coefficient $d = C/(\rho_0 H)$ gives the strength of the mechanical coupling between the ocean and the atmosphere and it was a key bifurcation parameter in [19].

The dynamic equations (3) and (4) are supplemented by temperature equations for the two subsystems. For the atmosphere,

$$\gamma_a \left(\frac{\partial T_a}{\partial t} + J(\psi_a, T_a) - \sigma \omega \frac{p}{R} \right) = -\lambda (T_a - T_o) + E_{a,R}, \quad (6)$$

with

$$E_{a,R} = \epsilon_a \sigma_B T_o^4 - 2\epsilon_a \sigma_B T_a^4 + R_a. \quad (7)$$

Table 2. List of parameters of the extratropical VDDG module.

Parameter (unit)	Value	Parameter (unit)	Value
$L_y = \pi L$ (km)	5.0×10^3	γ_o ($\text{J m}^{-2} \text{K}^{-1}$)	$4 \times 10^6 h$
f_0 (s^{-1})	1.032×10^{-4}	C_o (W m^{-2})	310
$n = 2L_y/L_x$	1.5	T_o^0 (K)	285
R_E (km)	6370	γ_a ($\text{J m}^{-2} \text{K}^{-1}$)	1.0×10^7
ϕ_0	$\pi/4$	C_a (W m^{-2})	$C_o/4$
g'	3.1×10^{-2}	ϵ_a	0.76
r (s^{-1})	1.0×10^{-7}	β ($\text{m}^{-1} \text{s}^{-1}$)	1.62×10^{-11}
H (m)	100	T_a^0 (K)	270
d (s^{-1})	$C/(\rho_o H)$	λ ($\text{W m}^{-2} \text{K}^{-1}$)	1004 C
k_d (s^{-1})	$(gC)/(\Delta p)$	R ($\text{J kg}^{-1} \text{K}^{-1}$)	287
k'_d (s^{-1})	$(gC)/(\Delta p)$	σ ($\text{J kg}^{-1} \text{Pa}^{-2}$)	2.16×10^{-6}
C ($\text{kg m}^{-2} \text{s}^{-1}$)	0.008		

Here R is the gas constant, ϵ_a the emissivity of the atmosphere, σ_B the Stefan–Boltzmann constant, R_a the shortwave radiation at the top of the atmosphere, ω the vertical velocity in pressure coordinates, and $\sigma = -(R/p)(\partial T_a/\partial p - 1/(\rho_a c_p))$ is the static stability, with p the pressure, ρ_a the air density, c_p the specific heat at constant pressure, and σ here is taken to be a constant. Note also that, thanks to the hydrostatic relation in pressure coordinates and the ideal gas relation $p = \rho_a R T_a$, the atmospheric temperature can be written as $T_a = -(p/R)f_0(\partial \psi_a/\partial p)$.

For the ocean,

$$\gamma_o \left(\frac{\partial T_o}{\partial t} + J(\psi_o, T_o) \right) = -\lambda(T_o - T_a) + E_R, \quad (8)$$

with

$$E_R = -\sigma_B T_o^4 + \epsilon_a \sigma_B T_a^4 + R_o. \quad (9)$$

Here R_o is the shortwave radiation entering the ocean, γ_o the heat capacity of the ocean, and λ is the inverse of the time scale associated with heat transfer between the ocean and the atmosphere, which includes both the latent and sensible heat fluxes. In fact, we assume that this combined heat transfer is proportional to the temperature difference between the atmosphere and the ocean.

The temperatures in both modules are linearized around a reference value in order to reduce the quartic terms of the energy balance equations (7) and (9) to linear terms, assuming that the temperature fluctuations are small. This modification helps one to reduce the number of terms on the right-hand side of the ordinary differential equations (6) and (8) when building the spectral low-order model.

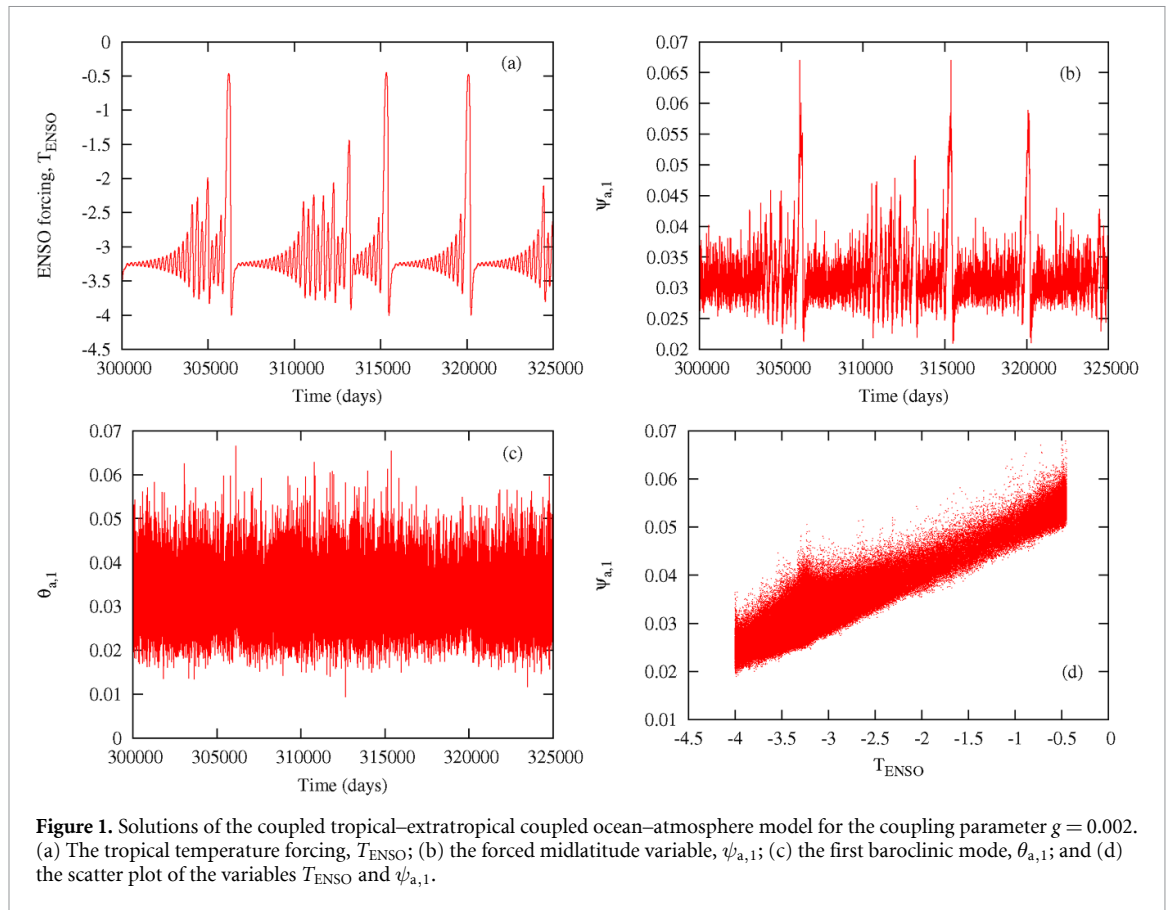
The model fields in both its atmosphere and its ocean are developed in Fourier series and truncated at a low order. The number of modes herein is fixed at 10 for the atmosphere and 8 for the ocean, leading to 20 ordinary differential equations for the former and 16 for the latter. This model configuration is the original VDDG one; see also [21]. The parameter values used in the present work are listed in table 2. In the configuration of table 2, there is no substantial LFV emerging in the extratropical component (see [12]), allowing for solely clarifying the impact of external LFV.

2.3. Modeling the tropical–extratropical interaction

[31] investigated the changes of extratropical wintertime cyclogenesis when El Niño or La Niña events are occurring in the tropical Pacific. They showed, in particular, that the background zonal-flow anomaly is more intense over the North Atlantic during La Niña, while it is stronger over the north Pacific during El Niño. This finding tells us that an important effect of the tropical forcing is to change the intensity of the zonal flow in either region, and that the impact of El Niño and La Niña differs from one region to the other. In order to mimic this dynamic effect in the extratropical VDDG model used here, we impose a direct linear forcing of the model's first barotropic atmospheric mode. It is this barotropic streamfunction mode that represents the intensity of the zonal flow within the atmosphere. Its dynamics is written as

$$\frac{d\psi_{a,1}}{dt} = f_1(\psi_{a,1}, \theta_{a,1}) + g\delta(x+y). \quad (10)$$

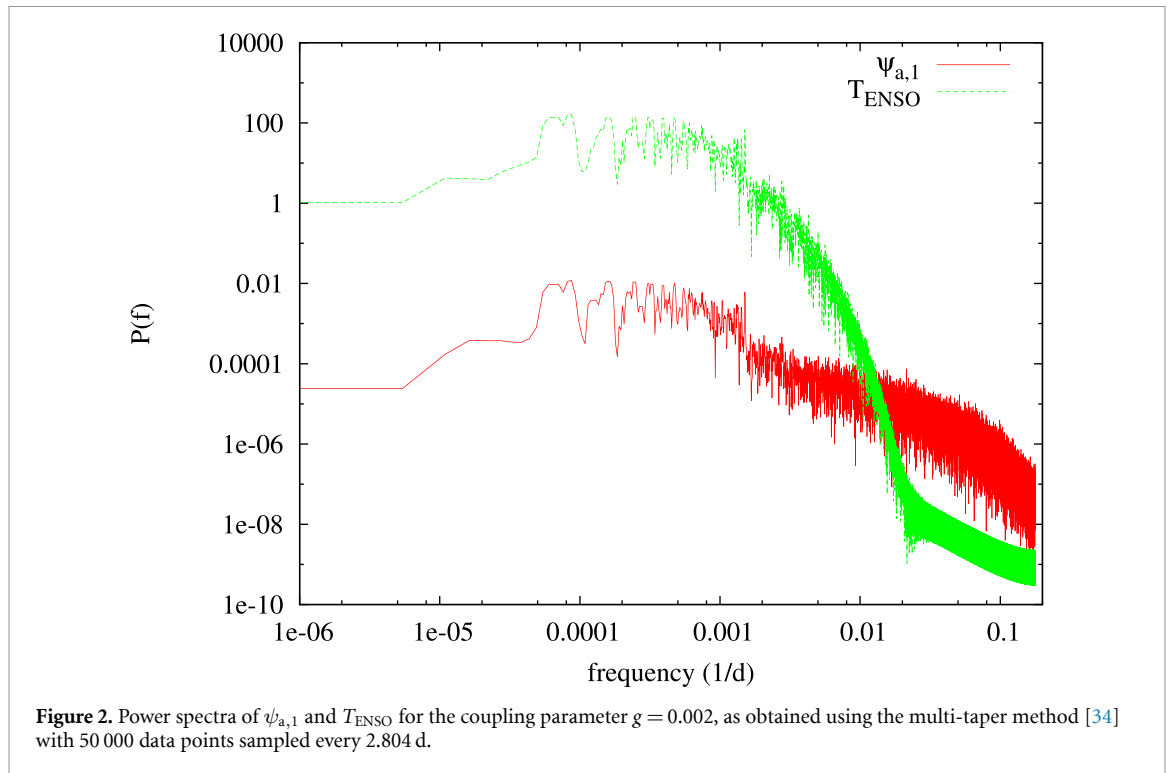
Here $f_1(\psi_{a,1}, \theta_{a,1})$ is the original right-hand side of the dynamical evolution (3a) of $\psi_{a,1}$; $\delta(x+y)$ represents the eastern tropical Pacific basin's temperature anomalies; and g scales the intensity of the tropical forcing.



Thus g represents the crucial forcing of the midlatitude VDDG model described in section 2.2 above by the ENSO module of section 2.1. In our setting, given a positive g -value, a positive, warm anomaly will induce an increase of $\psi_{a,1}$, and hence of the mean zonal flow, $U = -\psi_{a,1}\partial(\sqrt{2}\cos y)/\partial y$. This situation corresponds to the intensification of the zonal flow over the north Pacific during an El Niño. If, to the contrary, g is negative, this would correspond to an intensification during La Niña that mimics the ENSO effect over the north Atlantic. In the current analysis, we are focusing on one specific positive value of g providing a strong teleconnection between the tropics and the midlatitudes.

Figure 1 displays a typical trajectory of the idealized ENSO model for a coupling parameter of $g = 0.002$. Panel (a) shows the forcing trajectory of sea surface temperature in the east equatorial Pacific with a succession of strong and less strong El-Niño, and la Niña events, occurring in an irregular manner. The evolution of the first mode of the barotropic streamfunction, $\psi_{a,1}$, is shown in panel (b), indicating regular bursting associated with strong El-Niño events. Panel (c) shows the same type of evolution for the first mode of the baroclinic streamfunction, $\theta_{a,1}$, strongly related to the evolution of $\psi_{a,1}$. In this evolution, the bursting is not visible anymore, indicating a much lower influence of the tropical forcing than for $\psi_{a,1}$. Finally in panel (d), the relationship between the instantaneous values of $\psi_{a,1}$ and the temperature in the east part of the tropical ocean basin is displayed, indicating a strong teleconnection between the modeled tropical Pacific and the streamflow of the midlatitude model. The correlation between the two observables is equal to 0.914, a strong teleconnection between the two regions in this idealized modeling. If the tropical–extratropical coupling parameter g is modified, one can either increase or decrease the strength of these teleconnections. Such an impact will be addressed in the next section.

In order to further clarify the link between the tropical and extratropical systems, power spectra of $\psi_{a,1}$ and T_{ENSO} for the coupling parameter $g = 0.002$ are displayed in figure 2. For the forcing T_{ENSO} , the energy is concentrated at frequencies below 0.001, with a rapid drop at larger frequencies. For $\psi_{a,1}$, the spectrum is much flatter at high frequencies than for the forcing, indicating that a substantial amount of energy is contained at that frequencies. Interestingly a strong similarity of the spectra between frequencies of 10^{-5} and 0.002 is found, indicating the strong link between the forcing and $\psi_{a,1}$. Note that the broadband peak of the T_{ENSO} is obviously reflecting the chaotic nature of the dynamics, but we can isolate a few dominating peaks at about 30, 15, 11 and 5 years. The latter is the one familiar in many time series analysis of the ENSO evolution. The former ones may be emulating the long term behavior of ENSO which displays stronger El-Niño events on decadal and multi-decadal time scales [32, 33].



3. Predictability at midlatitudes

3.1. Experimental setup

The tropical–extratropical coupled system presented in section 2 allows for a clean analysis of the limits of predictability of the extratropical climate system forced by the tropics. As briefly mentioned in the previous section, the solution generated by the tropical model is chaotic, implying that the signal to be extracted also exhibits sensitivity to initial conditions as for the extratropics. The Lyapunov time scale of the tropical solution is of the order of 7 years, indicating a very slow increase of errors in time compatible with the dynamics of ENSO.

A very long control run of the model is first generated which provides the reference against which all forecasting experiments will be evaluated. This constitutes our truth. For the forecasting experiments, it is assumed that an estimate of the truth has been done at specific times along the reference trajectory with some uncertainty. This uncertainty is generated using random perturbations. We suppose that this uncertainty is coming from a uniform distribution for the variables in both the tropical region and at midlatitudes. It is also further assumed that we know this distribution exactly and one can therefore generate an appropriate ensemble forecasting system based on the same distribution as the one used to generate the uncertainty of the observations. The ensemble forecasts are therefore done as follows.

A first set of random perturbations mimicking the uncertainty on the initial conditions in the extratropics is introduced. The distribution used is a uniform distribution of mean 0 and range $[-5 \cdot 10^{-7} : 5 \cdot 10^{-7}]$. This amplitude is very small as compared with the amplitude of the variables (in non-dimensional units). Typically of the order of 0.001% of the variability of $\psi_{a,1}$. This mimics a situation for which the initial conditions are very well known in the extratropics, that will allow for having a clear picture of the different phases of the error dynamics and the skill of the model variables.

The tropical dynamics is also affected by initial condition errors, that will in turn affect the forecasts in the extratropics. In order to mimic this feature, a random initial error is also introduced in the initial conditions of the tropical model, generated from a uniform distribution of zero mean and an amplitude, PT , of either 0, 0.02 and 0.05, 0.10, 0.15 and 0.20. Thus the distribution is covering the domain $[-PT/2 : PT/2]$. The perturbation amplitudes are therefore ranging from 0% to 15% of the natural variability of the tropical model temperature, $x + y$, used to force midlatitudes.

As in many long-term forecasting systems, an ensemble of forecasts is generated starting from different initial conditions. The number, M , of such ensemble members will be modified in order to clarify their impact on the ensemble mean estimate. The initial conditions of these ensemble members are perturbed consistently with the uncertainties affecting the two models in order to generate a reliable forecast: once an

initial state is defined with the uncertainties mentioned above, random perturbations sampled from the same uniform distributions are generated and added to this initial state to produce each member of the ensemble.

For verification, a few usual metrics are computed: the correlation between the reference trajectory and the forecasts or the ensemble mean (referred as the correlation skill), and the mean square error (MSE). To get estimates that are independent of the initial conditions on the attractor of the coupled system, $N = 2000$ realizations are performed starting at different times along the reference trajectory.

3.2. Perfect teleconnection predictability

In order to illustrate the potential impact of the teleconnections introduced in this system on the skill of the solutions, let us first consider the experiments done without error in the initial conditions of the tropical forcing for values of the coupling parameter $g = 0$ and 0.002 . In other words, it is assumed that the forcing evolution is perfectly known, which should allow for exploiting optimally the teleconnections revealed in figure 1. The error in the initial states of the extratropical model is fixed as discussed in the previous section.

Figure 3(a) shows the correlation skill between the control integration (without initial condition errors) and single forecasts ($M = 1$) for variables $\psi_{a,1}$ and $\theta_{a,1}$ for $g = 0$ and $g = 0.002$. For $g = 0$, the correlation skill is completely lost after about 50 d. When the forcing is introduced with $g = 0.002$, the picture is similar for the variable $\theta_{a,1}$, while for variable $\psi_{a,1}$ the correlation skill is first quickly decreasing and then saturates around a value of about 0.82. Two general comments are in order here with the specific design of the tropical–extratropical model: (i) the teleconnection present between the forcing and $\psi_{a,1}$ induce a long term correlation skill of this variable with a plateau at a level defined by the strength of the teleconnection induced by the tropical forcing; and (ii) there is no obvious propagation of the teleconnection dependence to the baroclinic variable, $\theta_{a,1}$, strongly related to the dynamics of $\psi_{a,1}$. Although this type of consideration is not entirely new, it provides a key reference for the experiments that will be done next. In particular, the strong correlation between the reference and forecasting trajectories for $\psi_{a,1}$ reveals the strong potential of teleconnections. This correlation skill level for $g = 0.002$ of $\psi_{a,1}$ will be referred in the following as the *perfect teleconnection predictability* (PTP).

Figure 3(b) shows the PTP for various values of g from 0 to 0.003. It reveals that once g is increased, the PTP increases accordingly. It is however interesting to point to the fact that the level of correlation skill shown from, say, 100 to 500 d, is always smaller than the correlation between $\psi_{a,1}$ and T_{ENSO} : for $g = 0.0005$, the correlation is 0.50, while the level of the corresponding correlation skill in figure 3(b) is lower than 0.25. This reflects the complex interplay between the forcing and the forced variable. So the teleconnection as defined by the correlation between $\psi_{a,1}$ and T_{ENSO} is an upper bound of the actual correlation skill of $\psi_{a,1}$.

From figure 3(b), it is also interesting to note that whatever the value of g , the quick initial decrease of skill toward the plateau is very similar. The reason is that the short term predictability of the extratropical model is almost the same when measured by the first Lyapunov exponent for this range of values of g (see [12]).

3.3. Predictability for $M = 1$

Let us now focus on the case $g = 0.002$ and consider the more realistic situation for which there are some uncertainties in the initial conditions of the tropical forcing, but still with only one ensemble member $M = 1$. As the tropical model is chaotic, it also displays sensitivity to initial conditions that will affect in turn the extratropical forecasts.

Figure 4 displays the evolution of the MSE for several amplitudes of the perturbations of the initial states of the tropical model. On this doubly logarithmic scale, a first interesting information is the quadratic increase of the MSE for short lead times. This behavior is well documented and typical when model errors or boundary forcing errors are present [35–37]. Interestingly this error quickly amplifies suggesting that boundary forcing errors can considerably harm the forecasts in the extratropics whatever the quality of the initial conditions of the extratropical model. Another important information, is the level of saturation of the error which is reached when forcing errors are present: the error at long lead times is higher. Finally, the way it saturates from, say, 30 d to the end of the forecasts shows a complex feature related to the time scales of the forcing: a plateau is present between 30 and 100 d which is a period for which the difference between the forcing acting on the reference and the forecasting model is still small, and hence following the error evolution in the absence of any initial condition error of the tropical model; and then followed by an oscillating behavior associated with the typical oscillations found in the original tropical model dynamics. The specific sharp decrease of the error around 900 d needs further clarifications by investigating the detailed evolution of the distribution of the errors as a function of time on these time scales and beyond for various initial error amplitude in the forcing. This question will be addressed in the future.

Although the error evolution is an interesting quantity to analyze in particular for the short terms, the correlation skill is probably more relevant for the long term in order to clarify the impact of the teleconnections. In figure 5, the evolution of the correlation skill between the reference and the forecast of

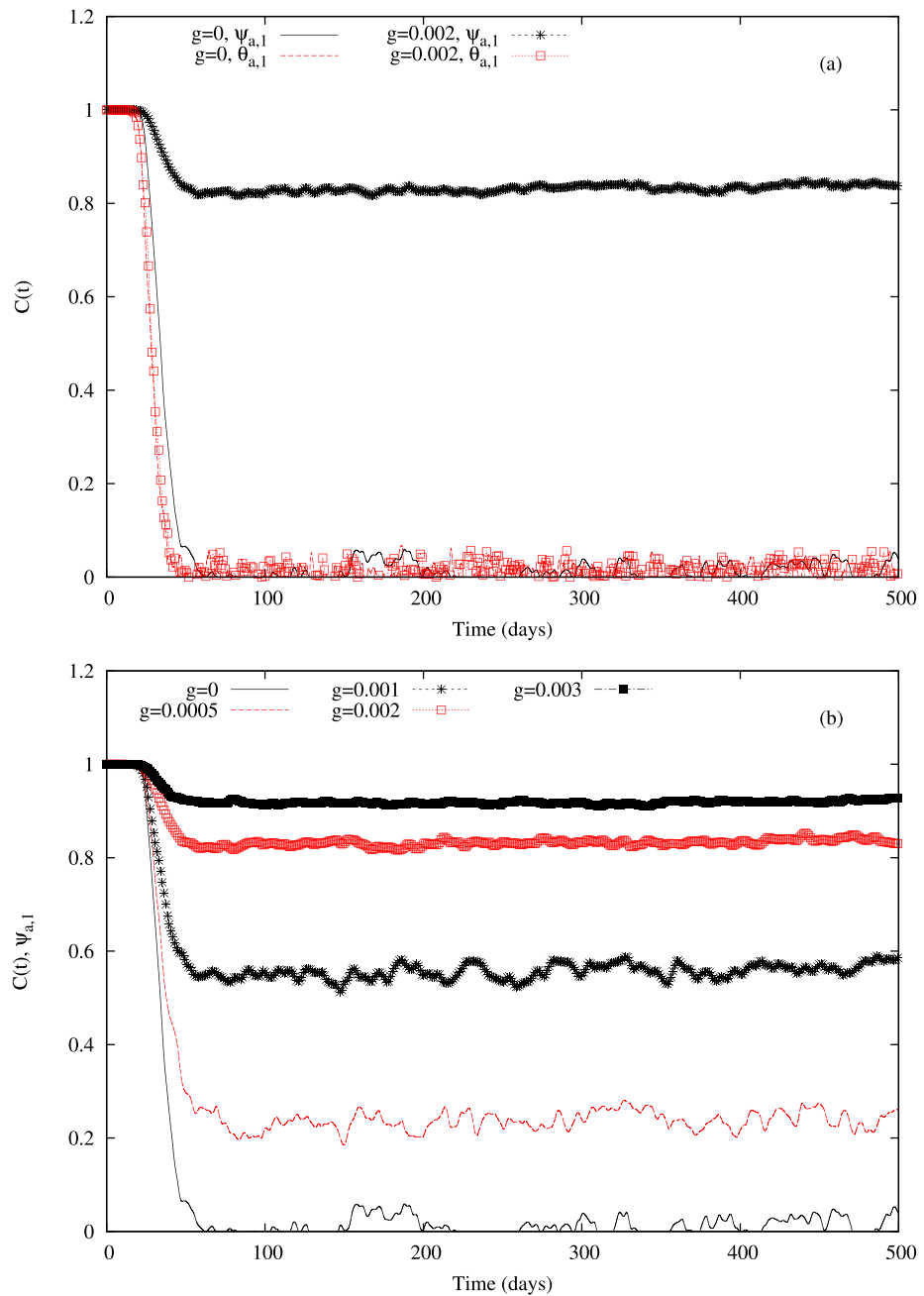


Figure 3. Correlation between the reference integration, viewed as perfect observations, and the ensemble mean of forecasts for (a) variables ψ_1 and θ_1 for $g = 0$, and $g = 0.002$ and (b) variable ψ_1 for $g = 0, 0.0005, 0.001, 0.002$ and 0.003 . The ensemble size is fixed to $M = 1$, hence corresponding to single deterministic forecasts.

the variable $\psi_{a,1}$ with or without errors in the initial conditions of the tropical model, is displayed. After a quick decrease to the level of the PTP experiment (black continuous line), the correlation skill persists around that level for a few days or weeks depending on the amplitude of the error in the initial conditions of the tropical forcing. It then drops to a lower level that also depends on the amplitude of the initial error. Two important messages here: (i) the teleconnection skill can never be reached on the long term basis when error in the initial conditions are present in the tropical model forcing; (ii) the ability to keep skill on long lead times depends on the amplitude of the errors in the initial conditions of the tropical model.

3.4. Impact of ensemble averaging

A first approach to improve the skill is to generate an ensemble of runs starting from different initial conditions and to extract the ensemble mean. It has been shown that the skill is improved even if a very small number of ensemble members is used [38, 39].

Let us start by investigating the error evolution for different values of M for the case for which the initial condition error amplitude of the tropical model is fixed to $PT = 0.05$. The results are displayed in figure 6.

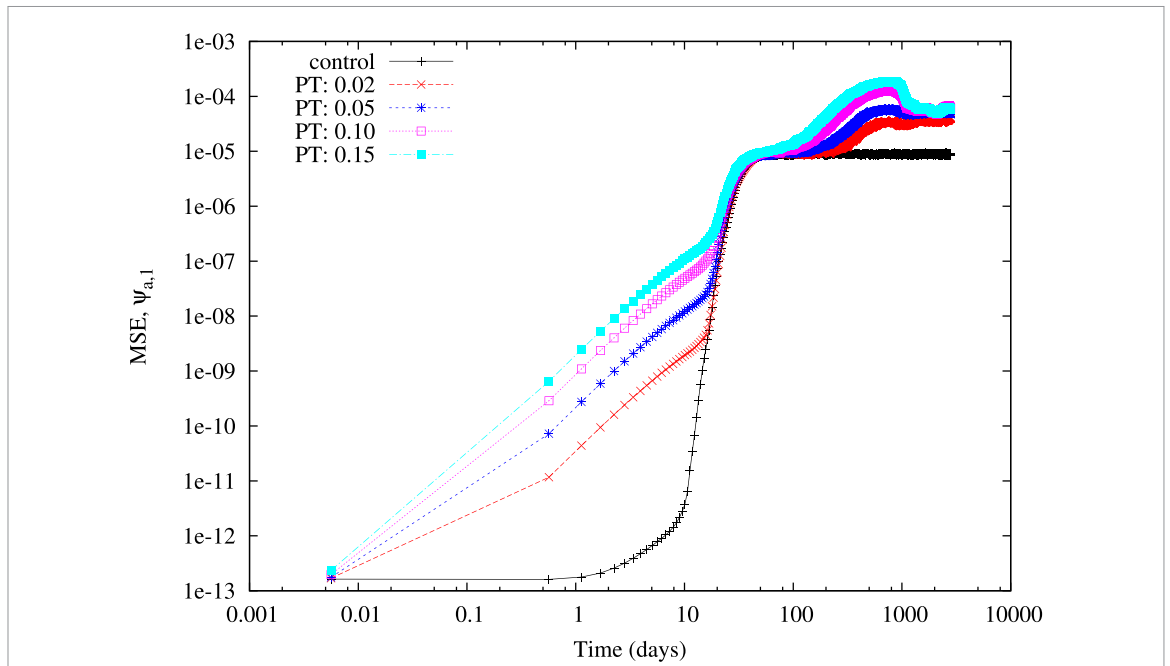


Figure 4. MSE evolution for the variable $\psi_{a,1}$ under the influence of tropical forcing, affected by different initial condition error amplitudes, $PT = 0, 0.02, 0.05, 0.10, 0.15$.

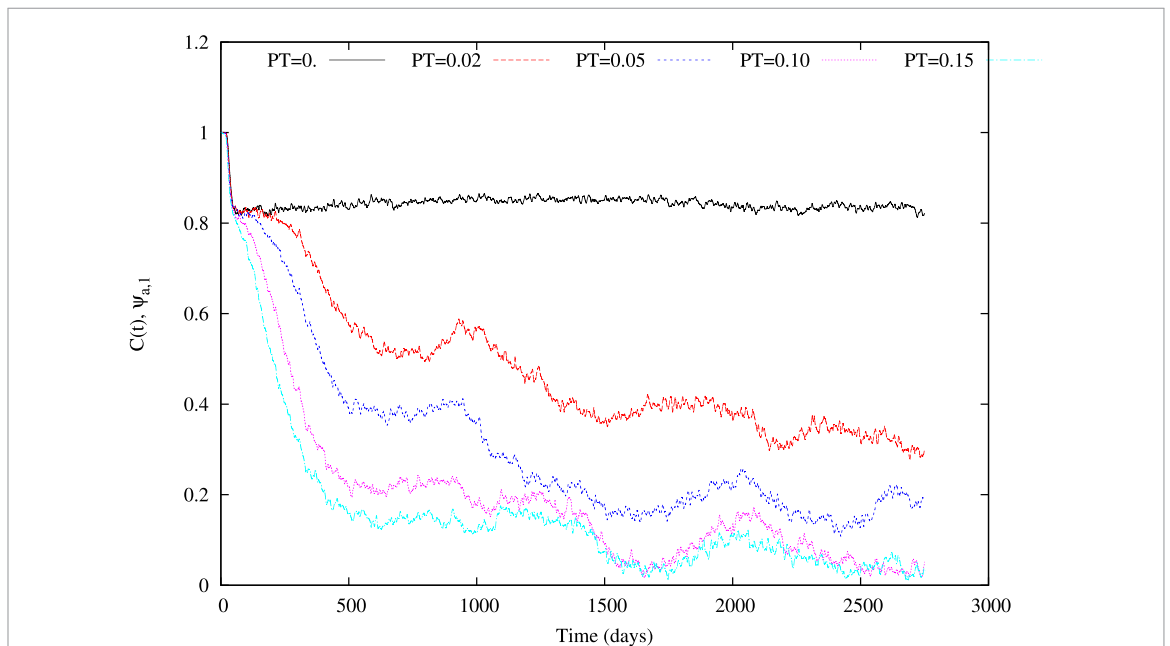
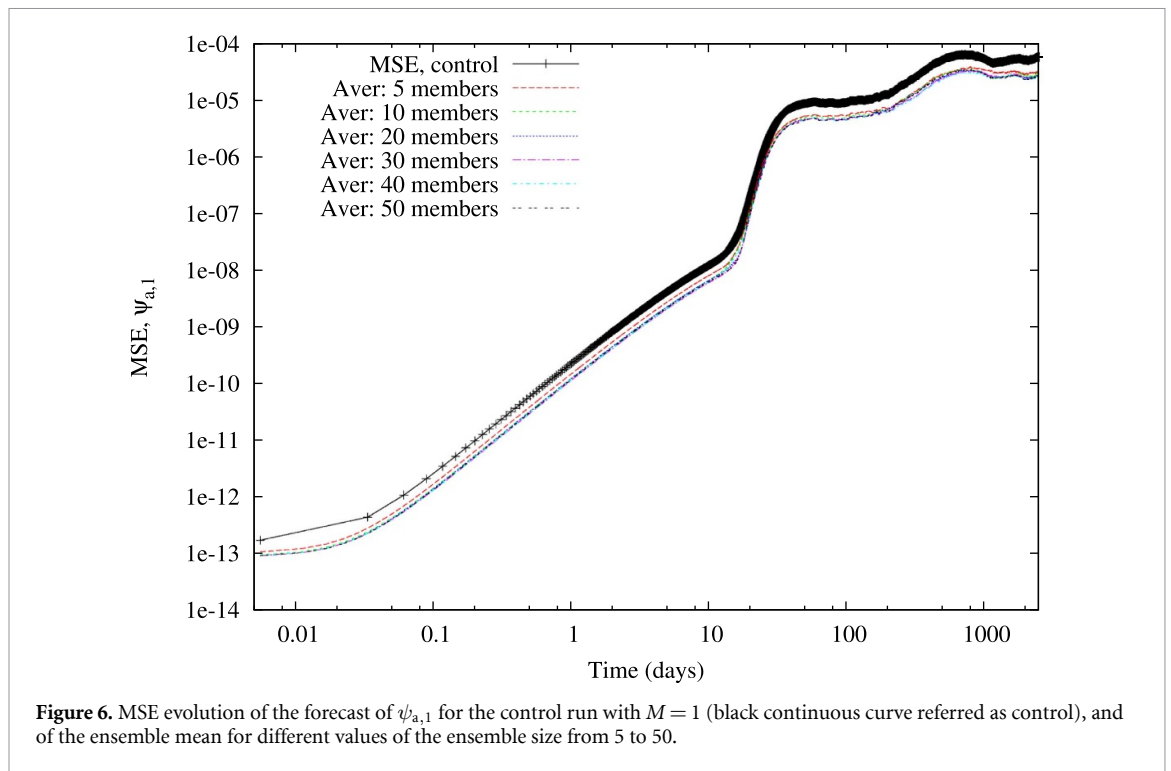


Figure 5. Evolution of the correlation skill for $M = 1$ for different amplitudes of the errors introduced in the initial conditions of the tropical model.

The key information that can be extracted is that even with 5–10 members, the main improvement that can be obtained through averaging is reached: little improvements can be obtained going beyond that order. This was already pointed out in [38] in an intermediate complexity model with much more degrees of freedom.

This impact of ensemble averaging on the correlation skill is then illustrated in figure 7 for (a) $\psi_{a,1}$ with a perturbation amplitude of $PT = 0.02$, and (b) with a perturbation amplitude of $PT = 0.05$. In these plots, the correlation skill corresponding to the PTP is also displayed, as well as the case with $M = 1$.

A first remark is that the correlation skill between the reference and the ensemble mean forecasts is still lower than PTP for long lead times when initial condition perturbations are introduced in the forecasting model of the forcing. Moreover when the number of members is increased, the quality of the forecast is increased, but already ten members are enough to reach the optimal skill. The latter result is consistent with the fact that the ensemble mean is rapidly converging to its asymptotic value as discussed in [38].



A second important result is the improvement of the correlation skill when the ensemble mean is used as forecast between 50 and about 300 d. The correlation skill is now reaching values close to the teleconnection correlation between the forcing and the variable. In other words, the ensemble averaging is properly filtering the fast weather variability around the mean. The ensemble mean is here an appropriate approach to isolate the signal present in the variable $\psi_{a,1}$.

For the variable $\theta_{a,1}$, the skill decreases quickly and is similar whatever the initial condition error in the tropical model as illustrated in figure 8, suggesting the weak sensitivity of this variable to the external forcing. Note however that there is some improvements by taking ensemble averages in the phase of quick decrease of the skill around 30–40 d, even with a small number of ensemble members.

In the last decades, many studies have tried to evaluate the potential forecasting skill of climate forecasting models, and compared it to the actual forecast skill [40–42]. The potential forecasting skill is the correlation between the ensemble mean and any member of the ensemble. In this context if the model is perfect and if the model is properly initialized, the potential predictability should be equal to the actual predictability.

In fact even if the model is properly representing the reference evolution, a discrepancy between the actual skill and the potential skill is found in the current experiment. This is illustrated in figure 9. The potential skill is larger than the actual skill, except when there is no initial condition errors in the tropical model forecasts (black curves). This feature in the current coupled tropical–extratropical model may only be understood by the fact that even if perturbing randomly and symmetrically the initial conditions around the observations (and hence the reference) in the tropical model, a forecasting bias is emerging (not shown). This forecasting bias is most probably due to the way the solutions of the forecasting model are converging back to the model’s attractor. Such feature is very subtle and is worth addressing further in a future study by analyzing the temporal properties of these transient trajectories, and to propose new approaches for perturbing the model more consistent with the natural dynamics of the reference system as discussed for instance in details in [43] or using analog initialization as in [44].

3.5. Impact of temporal averaging

Ensemble averages are often used to improve the estimate the future state of the system. As shown in the previous section, this is indeed interesting and the correlation skill score can be improved to a certain extent. But once the number of members is large enough, no improvement is obtained, this number being related to the quick convergence of the ensemble mean to its asymptotic value.

Another way to extract the signal from the forecasts is often to take temporal averages (running means). This question has been addressed in several papers in the past, in particular showing that the short term dynamics of the error as described by the dominant Lyapunov exponent is the same as for instantaneous fields [45–47]. The main modification that can then be expected is for long term forecasts as discussed in

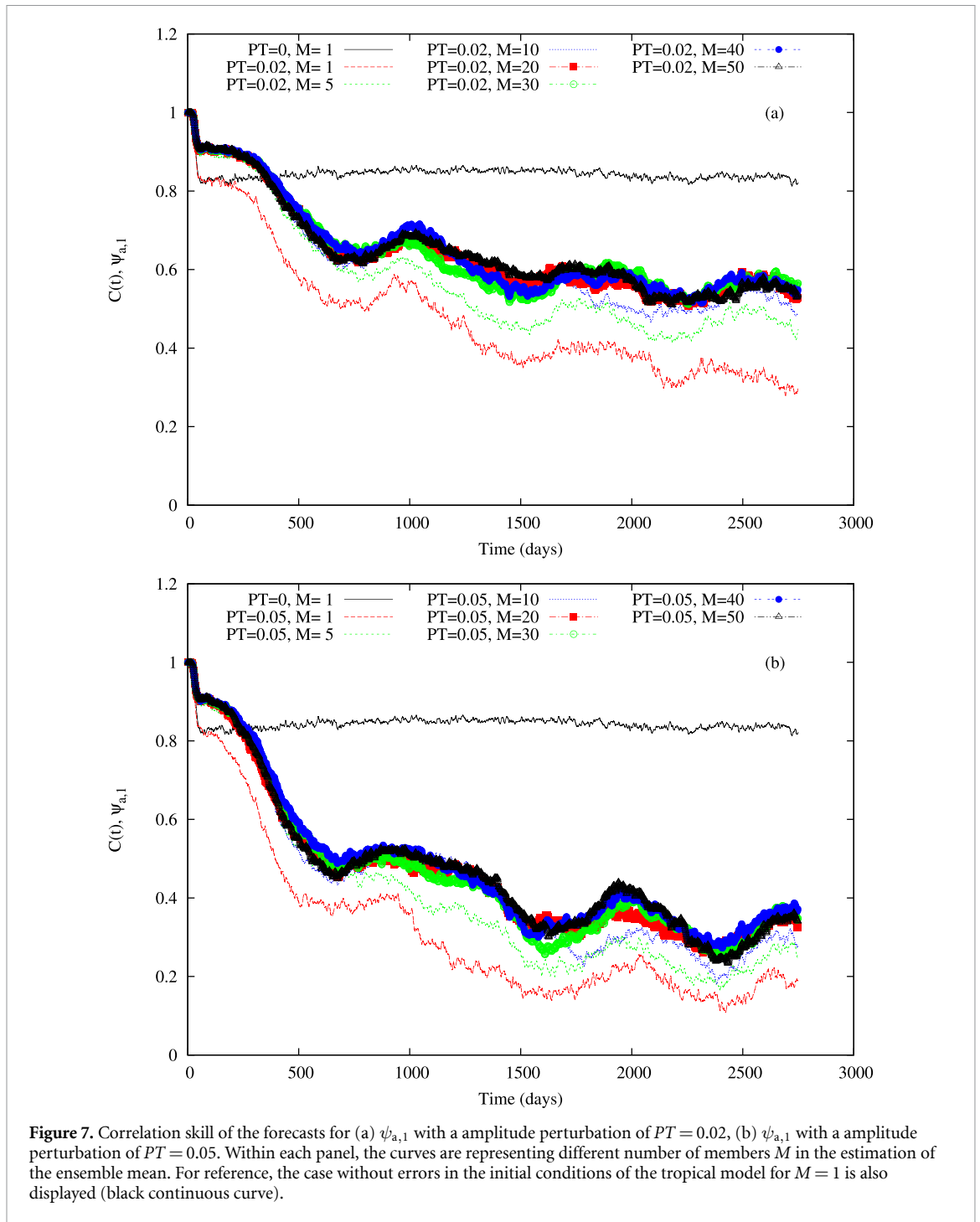


Figure 7. Correlation skill of the forecasts for (a) $\psi_{a,1}$ with a amplitude perturbation of $PT = 0.02$, (b) $\psi_{a,1}$ with a amplitude perturbation of $PT = 0.05$. Within each panel, the curves are representing different number of members M in the estimation of the ensemble mean. For reference, the case without errors in the initial conditions of the tropical model for $M = 1$ is also displayed (black continuous curve).

[48], but the gains are very low when investigating atmosphere-only models [49]. We also explored this question in the context of the tropical–extratropical coupled model to clarify the impact on the time averaging in the extraction of the signal associated with the tropical forcing.

Figure 10 is displaying the different MSE curves for the ensemble mean with $M = 5$ for the temporal averages of the variable $\psi_{a,1}$. The averages have been performed from about 5 d to 60 d. Note that the lead time, time = 0 d, is taken at the end of the averaging period T , so that time = 0 on the figure is associated with the averaging over T days of the original forecast. Four different phases can be found in the evolution of the error: first an overall increase of the MSE for short times associated with the averaging of successive situations displaying large errors as compared with the reference for longer lead times; a second phase during which the MSE amplitude is decreasing when T becomes large (from lead times of 25–200 d); a third phase of rapid growth (from 200 d to 400 d) for which averaging does not change the MSE amplitude; and finally a phase (after 400 d) for which the MSE amplitude again decreases for large values of T . This complicated dependence reflects that time averaging may indeed reduce the variance, and hence the error, of the processes

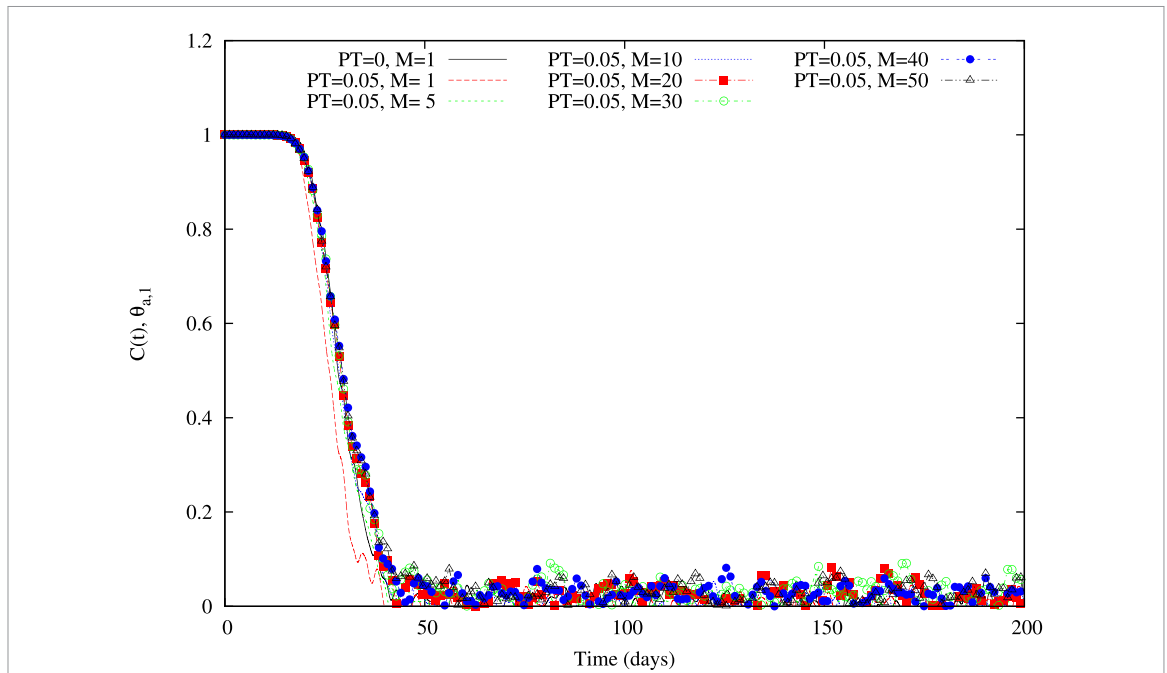


Figure 8. As in figure 7 but for the variable $\theta_{a,1}$ with an amplitude perturbation of $PT = 0.05$. The curves are representing different number of members M in the estimation of the ensemble mean. For reference the case without errors in the initial conditions of the tropical model is also displayed (black continuous curve).

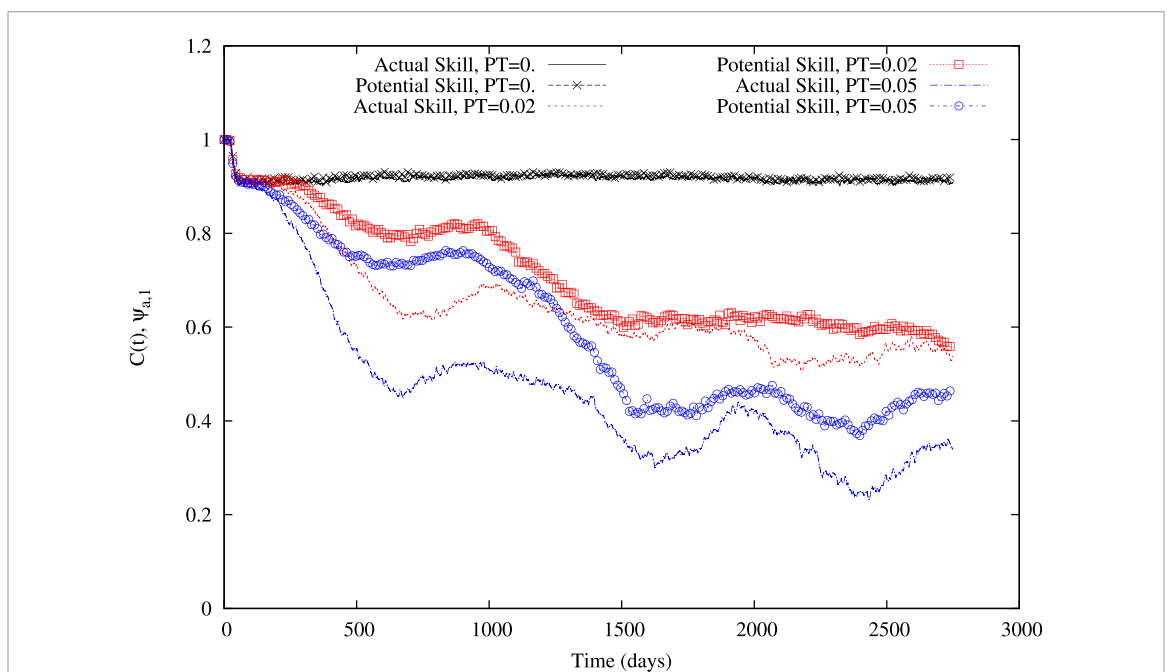
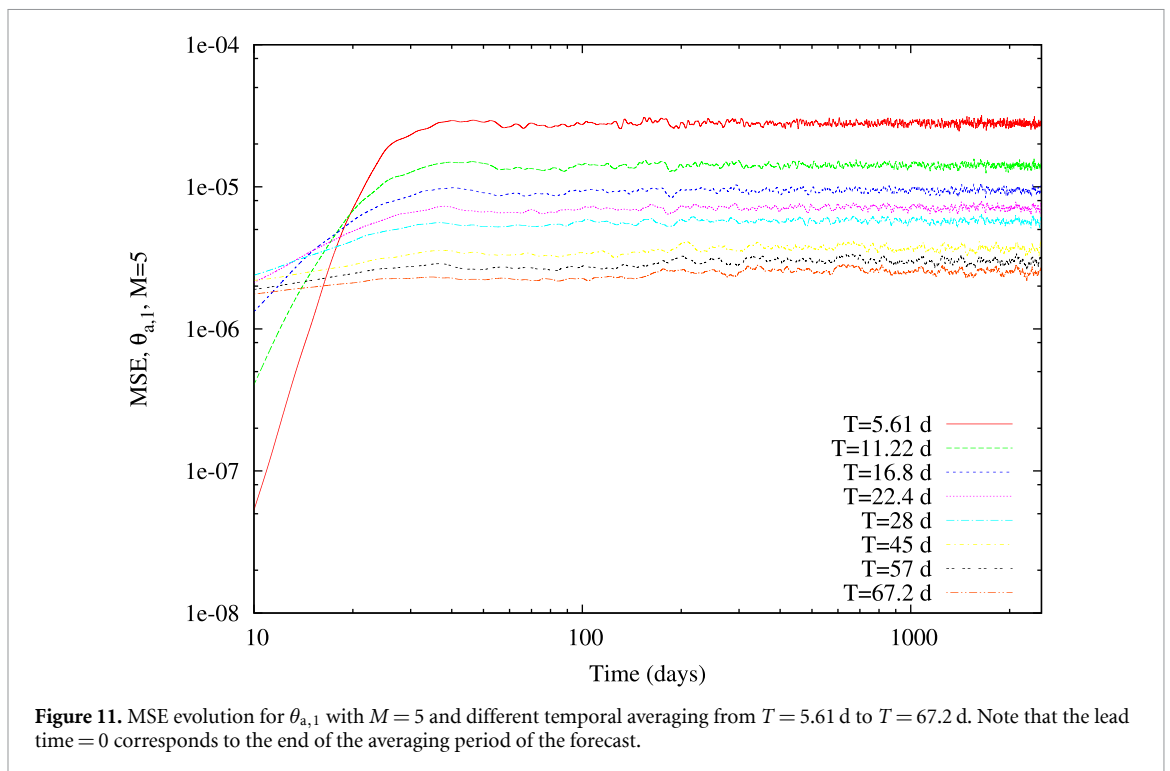
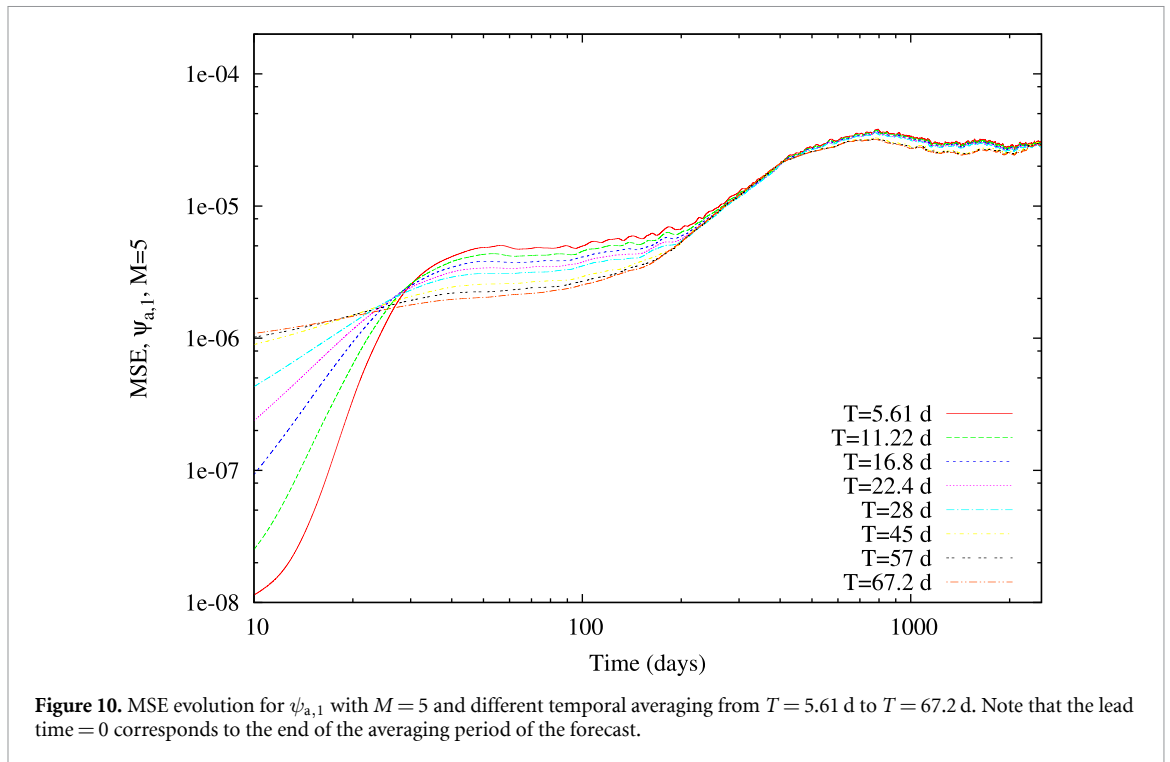


Figure 9. Comparison of the actual forecasting skill of the ensemble mean and the potential predictability—as defined by the skill of the ensemble mean in forecasting any of the member of the ensemble. Three cases are displayed with or without error in the initial conditions of the tropical model.

but not uniformly for all time scales. This aspect was already amply discussed in [45], and shows up here in different responses of the MSE phases to averaging. This differential behavior as a function of the phase does not however shows up for $\theta_{a,1}$ as illustrated in figure 11 with a constant decrease of the MSE saturation level as a function of time averaging. As $\theta_{a,1}$ is much less affected by the forcing than $\psi_{a,1}$, this differential behavior for $\psi_{a,1}$ could be associated with the action of the tropical forcing.

Another very useful view of what is happening while taking temporal averaging is to evaluate the changes in the correlation skill. In figure 12, the evolution of the correlation skill for the ensemble mean of five members ($M = 5$) of $\psi_{a,1}$ without time averaging, and with three different time averages of 11.2, 33 and 67.2 d. A small gain of averaging is found between 50 and 300 day lead times, suggesting the usefulness of this



averaging at such lead times. If now one looks at the corresponding figure for $\theta_{a,1}$ (figure 13), the picture is very different. Although the instantaneous quantities, with or without ensemble averaging, do not show skill beyond 40 d, the temporal average allows for getting skill of this observable at long lead times: for the temporal averaging of 67.2 d, a correlation skill of the order of 0.2 is found up to almost 1000 d. This suggests that the temporal averaging is appropriately removing the high frequency variability of $\theta_{a,1}$ and isolate the signal associated with the influence of the tropical forcing.

To sum up, temporal averages can be very helpful in extracting the skill of observables influenced by external forcing signals, even when the teleconnections are weak.

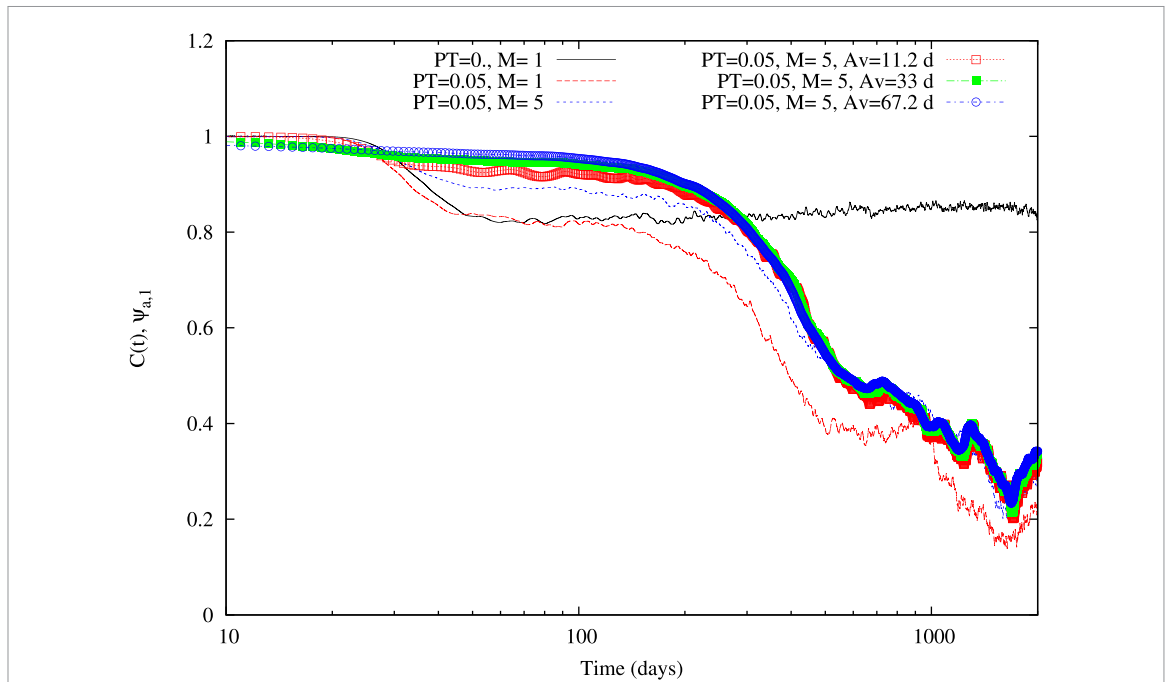


Figure 12. Evolution of the correlation skill for $\psi_{a,1}$ for various combinations of averaging (ensemble and/or in time).

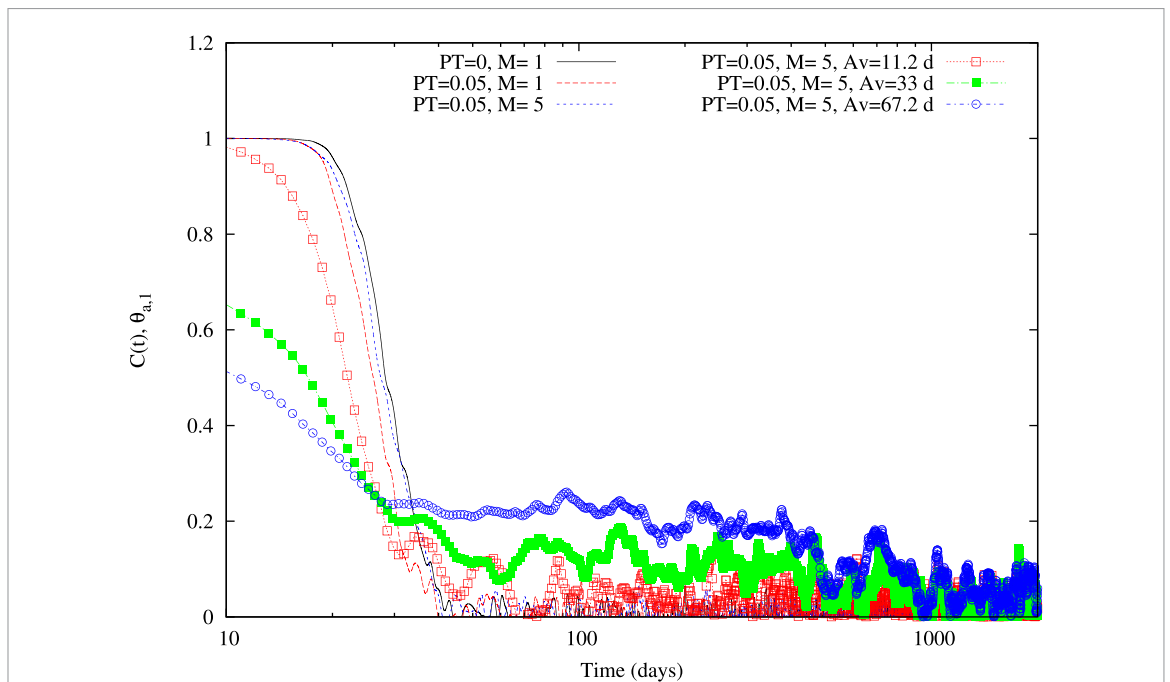


Figure 13. Evolution of the correlation skill for $\theta_{a,1}$ for various combinations of averaging (ensemble and/or in time).

4. Conclusions

LFV coming from the presence of an external slowly-evolving forcing are often isolated through teleconnections. In the present work, we have investigated in an idealized context the impact of the presence of teleconnections between the tropics and the extratropics on the limits of predictability of the extratropical fields. This has been done in a coupled tropical–extratropical model that was recently built to evaluate the emergence of LFV in the extratropics and the properties of the corresponding pullback attractors [12].

A highly idealized twin experiment was performed by running the coupled tropical–extratropical model with initial condition errors for both components of the system, and comparing its forecasts to a long reference run. A few generic properties were found:

- If there is no error in the initial conditions of the tropical model, the forced variable, here the first barotropic atmospheric mode, shows a skill on very long time scales thanks to the slowly-varying external forcing (which is in this case the same for the model forecast and the reference).
- When errors in the initial conditions are present, the correlation skill is considerably degraded at interannual lead times. The degradation of skill also depends on the amplitude of the initial condition errors in the tropics, suggesting that accurate initial conditions are necessary to get the full potential of teleconnections.
- Ensemble averaging may improve the quality of the forecasts, but the number of members necessary to reach an appropriate skill does not need to be large: 5–10 members are enough in this perfect model framework.
- Temporal averaging can also improve the quality of the forecasts (at the expense of course of being able to forecast extreme events), in particular when the forcing affects weakly the observable under interest. In the current context, the first baroclinic mode shows a very weak teleconnection (correlation) with the tropical forcing, and when averaging, a strong correlation skill is emerging.

This work also showed that even if the model is perfect and the initial observation distribution is known, the actual correlation skill of a forecast is always less or equal than the potential correlation skill as defined using the forecasting model itself only. This feature is very subtle and is most probably associated with the way the model forecasts are converging back to the system's attractor. This attractor is the same as the reference, but the path to converge to it is generating a forecasting bias which reduces the actual correlation skill. This suggests that appropriate initial conditions of the tropical model generating the forcing should be looked for, allowing for reducing this bias. This will be the subject of a future work along the lines of [43].

In the current work, the LFV is introduced through a one way external forcing from the tropics to the midlatitudes. Things become more complicated when part of the LFV is generated intrinsically in the forced system as for instance in [50] or when the forcing is interacting in a complicated way with the intrinsic LFV like in [12]. In both cases, the mean may lose significance, and a full probability distribution is then necessary to characterize the dynamics of the reference system. Further investigations of such complex interactions are worth performing in the future.

Finally this problem should also be tackled in the context of a more realistic model for which the initial conditions in the tropical domain should be modified in order to clarify how well we can exploit the teleconnections for prediction purposes. This will also be the subject of a future work.

Data availability statement

The data cannot be made publicly available upon publication because they are not available in a format that is sufficiently accessible or reusable by other researchers. The data that support the findings of this study are available upon reasonable request from the authors.

Acknowledgments

This work is supported by the Belgian Policy Office under Grant B2/20E/P1/ROADMAP, a contribution to the ROADMAP project of the JPI-Climate-JPI-Ocean research activities.

ORCID iD

Stéphane Vannitsem  <https://orcid.org/0000-0002-1734-1042>

References

- [1] Philander S G H 1990 *El Niño and the Southern Oscillation* (Academic)
- [2] Alexander M A, Bladé I, Newman M, Lanzante J R, Lau N-C and Scott J D 2002 The atmospheric bridge: the influence of ENSO teleconnections on air-sea interaction over the global oceans *J. Clim.* **15** 2205–31
- [3] Hoerling M P and Kumar A 2002 Atmospheric response patterns associated with tropical forcing *J. Clim.* **15** 2184–203
- [4] Stan C, Straus D M, Frederiksen J S, Lin H, Maloney E D and Schumacher C 2017 Review of tropical-extratropical teleconnections on intraseasonal time scales *Rev. Geophys.* **55** 902–37
- [5] Yeh S-W *et al* 2018 ENSO atmospheric teleconnections and their response to greenhouse gas forcing *Rev. Geophys.* **56** 185–206
- [6] Mosedale T J, Stephenson D B, Collins M and Mills T C 2006 Granger causality of coupled climate processes: ocean feedback on the North Atlantic Oscillation *J. Clim.* **19** 1182–94
- [7] Paluš M, Krakovská A, Jakubík J and Chvosteková M 2018 Causality, dynamical systems and the arrow of time *Chaos* **28** 075307
- [8] Runge J *et al* 2019 Inferring causation from time series in earth system sciences *Nat. Commun.* **10** 2553
- [9] Vannitsem S and Liang X S 2022 Dynamical dependencies at monthly and interannual time scales in the climate system: study of the North Pacific and Atlantic regions *Tellus A* **74** 141–58
- [10] Kumar A and Hoerling M P 1995 Prospects and limitations of seasonal atmospheric GCM predictions *Bull. Am. Meteorol. Soc.* **76** 335–45

- [11] Nidheesh A G, Lengaigne M, Vialard J, Izumo T, Unnikrishnan A S and Cassou C H 2017 Influence of ENSO on the Pacific decadal oscillation in CMIP models *Clim. Dyn.* **49** 3309–26
- [12] Vannitsem S, Demaeyer J and Ghil M 2021 Extratropical low-frequency variability with ENSO forcing: a reduced-order coupled model study *J. Adv. Model. Earth Syst.* **13** e2021MS002530
- [13] Timmermann A, Jin F-F and Abshagen J 2003 A nonlinear theory for El Niño bursting *J. Atmos. Sci.* **60** 152–65
- [14] Vannitsem S 2015 The role of the ocean mixed layer on the development of the North Atlantic Oscillation: a dynamical system's perspective *Geophys. Res. Lett.* **42** 8615–23
- [15] Jin F-F 1996 Tropical ocean-atmosphere interaction, the Pacific cold tongue and the El-Niño-Southern Oscillation *Science* **274** 76–78
- [16] Jin F-F 1997 An equatorial ocean recharge paradigm for ENSO. Part I: conceptual model *J. Atmos. Sci.* **54** 811–29
- [17] An S-I and Jin F-F 2004 Nonlinearity and asymmetry of ENSO *J. Clim.* **17** 2399–412
- [18] Roberts A, Guckenheimer J, Widiasih E, Timmermann A and Jones C K R T 2016 Mixed-mode oscillations of El Niño-Southern Oscillation *J. Atmos. Sci.* **73** 1755–66
- [19] Vannitsem S, Demaeyer J, De Cruz L and Ghil M 2015 Low-frequency variability and heat transport in a low-order nonlinear coupled ocean-atmosphere model *Physica D* **309** 71–85
- [20] De Cruz L, Demaeyer J and Vannitsem S 2016 The modular arbitrary-order ocean-atmosphere model: MAOOAM v1.0 *Geosci. Mod. Dev.* **9** 2793–808
- [21] Vannitsem S 2017 Predictability of large-scale atmospheric motions: Lyapunov exponents and error dynamics *Chaos* **27** 32101
- [22] Vannitsem S and Lucarini V 2016 Statistical and dynamical properties of covariant Lyapunov vectors in a coupled atmosphere-ocean model—multiscale effects, geometric degeneracy and error dynamics *J. Phys. A* **49** 224001
- [23] De Cruz L, Schubert S, Demaeyer J, Lucarini V and Vannitsem S 2018 Exploring the Lyapunov instability properties of high-dimensional atmospheric and climate models *Nonlinear Process. Geophys.* **25** 387–412
- [24] Demaeyer J and Vannitsem S 2017 Stochastic parametrization of subgrid-scale processes in coupled ocean-atmosphere systems: benefits and limitations of response theory *Q. J. R. Meteorol. Soc.* **143** 881–96
- [25] Demaeyer J and Vannitsem S 2018 Comparison of stochastic parameterizations in the framework of a coupled ocean-atmosphere model *Nonlinear Process. Geophys.* **25** 605–31
- [26] Penny S G, Bach E, Bhargava K, Chang C-C, Da C, Sun L and Yoshida T 2019 Strongly coupled data assimilation in multiscale media: experiments using a quasi-geostrophic coupled model *J. Adv. Model. Earth Syst.* **6** 1803–29
- [27] Tondeur M, Carrassi A, Vannitsem S and Bocquet M 2020 On temporal scale separation in coupled data assimilation with the ensemble Kalman filter *J. Stat. Phys.* **179** 1161–85
- [28] Carrassi A, Grudzien C, Bocquet M, Demaeyer J, Raanes P and Vannitsem S 2022 Data assimilation for chaotic systems *Data Assimilation for Atmospheric, Oceanic and Hydrological Applications* ed S-K Park and X Liang (Springer Science & Business Media)
- [29] Gill A E 1982 *Atmosphere-Ocean Dynamics* (Academic)
- [30] Pedlosky J 1987 *Geophysical Fluid Dynamics* 2nd edn (Springer)
- [31] Schemm S, Riviére G, Ciasto L M and Li C 2018 Extratropical cyclogenesis changes in connection with tropospheric ENSO teleconnections to the North Atlantic: role of stationary and transient waves *J. Atmos. Sci.* **75** 3943–64
- [32] Wittenberg A T 2009 Are historical records sufficient to constrain ENSO simulations? *Geophys. Res. Lett.* **36** L12702
- [33] Guckenheimer J, Timmermann A, Dijkstra H and Roberts A 2017 (Un)predictability of strong El Niño events *Dyn. Stat. Clim. Syst.* **2** dzx004
- [34] Ghil M *et al* 2002 Advanced spectral methods for climatic time series *Rev. Geophys.* **40** 41
- [35] Vannitsem S and Toth Z 2002 Short-term dynamics of model errors *J. Atmos. Sci.* **59** 2594–604
- [36] Nicolis C 2003 Dynamics of model error: some generic features *J. Atmos. Sci.* **60** 2208–18
- [37] Nicolis C 2007 Dynamics of model error: the role of the boundary conditions *J. Atmos. Sci.* **64** 204–15
- [38] Houtekamer P L and Derome J 1995 Methods for ensemble prediction *Mon. Weather Rev.* **123** 2181–96
- [39] Ehrendorfer M 1997 Predicting the uncertainty of numerical weather forecasts: a review *Meteorol. Z.* **6** 147–83
- [40] Kumar A, Peng P and Chen M 2014 Is there a relationship between potential and actual skill? *Mon. Weather Rev.* **142** 2220–7
- [41] Imada Y and Kawase H 2021 Potential seasonal predictability of the risk of local rainfall extremes estimated using high-resolution large ensemble simulations *Geophys. Res. Lett.* **48** e2021GL096236
- [42] Yang D, Tang Y, Yang X Q, Song X, Tan X, Wu Y, Yan X, Liu T and Sun X 2023 Probabilistic versus deterministic potential seasonal climate predictability under the perfect-model framework *Clim. Dyn.* **61** 4429–47
- [43] Demaeyer J, Penny S G and Vannitsem S 2022 Identifying efficient ensemble perturbations for initializing subseasonal-to-seasonal prediction *J. Adv. Model. Earth Syst.* **14** e2021MS002828
- [44] Li S, Rong X, Liu Y, Liu Z and Fraedrich K 2013 Dynamic analogue initialization for ensemble forecasting *Adv. Atmos. Sci.* **30** 1406–20
- [45] Nicolis C and Nicolis G 1995 From short-scale atmospheric variability to global climate dynamics: toward a systematic theory of averaging *J. Atmos. Sci.* **52** 1903–13
- [46] Vannitsem S and Nicolis C 1997 Lyapunov vectors and error growth patterns in a t21l3 quasigeostrophic model *J. Atmos. Sci.* **54** 347–61
- [47] Vannitsem S and Nicolis C 1998 Dynamics of fine-scale variables versus averaged observables in a t21l3 quasi-geostrophic model *Q. J. R. Meteorol. Soc.* **124** 2201–26
- [48] Roads J O 1987 Predictability in the extended range *J. Atmos. Sci.* **44** 3495–527
- [49] Tribbia J J and Baumhefner D P 1988 Estimates of the predictability of low-frequency variability with a spectral general circulation model *J. Atmos. Sci.* **45** 2306–18
- [50] Pierini S 2020 Statistical significance of small ensembles of simulations and detection of the internal climate variability: an excitable ocean system case study *J. Stat. Phys.* **179** 1475–95